

3-D Dynamic Analysis of Precariously Balanced Rocks Under Earthquake Excitation

S. Veeraraghavan & S. Krishnan

California Institute of Technology, USA



15 WCEE
LISBOA 2012

SUMMARY:

Hundreds of Precariously Balanced Rocks (PBRs) exist in California. Since these rocks have been precariously placed for thousands of years, they can help in constraining the range of PGV (peak ground velocity) and frequency content of the ground motions that could not have occurred at this location during the time that the rock has been precariously positioned. We are developing 3-D models (with accurate rock-pedestal contact interface) of some of the PBRs that have been imaged using Terrestrial Laser Scanning (TLS) techniques. We use Rigid body dynamics to solve for the dynamic response of the rock models subjected to idealized and earthquake ground motions intensities to arrive at probabilistic constraints on region-wide ground shaking intensity by combining the results of this study with cosmogenic dating of these rocks. Such analyses could help quantify seismic hazards and validate ground motion simulations.

Keywords: Precariously Balanced Rocks, Rigid body dynamics, Housner's block

1. INTRODUCTION

There are several precariously balanced rocks (PBRs) in the western US located on hill-sides and cliffs. Many of these rocks have evolved naturally and have been in their present configuration for thousands of years (Brune, 1996; Bell et al., 1998). To constrain the amount of time the rocks have been precarious, cosmogenic dating of the pedestal, rock and other surfaces on the surrounding landscape have been conducted (Hudnut et al., 2009). Brune conducted several road surveys in Southern California and Nevada and cataloged hundreds of precariously balanced rocks (Brune, 1996; Brune et al., 2006). These rocks are classified into two categories using a rough estimate of their quasi-static toppling acceleration (i.e., the minimum constant ground acceleration required to overturn the rock). An estimate of this acceleration can be obtained from pictures of the rock or from tilt tests, wherein the force required to tilt the rock until it is balanced on its outermost contact point is measured. If the quasi-static acceleration is between 0.1-0.3g, the rock is precariously balanced; else if it is between 0.3-0.5g, it is semi-precariously balanced rock. The presence of zones of PBRs thus indicates that no strong ground shaking has recently occurred in those areas, contradicting the published ground motion maps at least for some areas. An example of a PBR is the Benton rock [Fig. 1.1], which is an approximately 2 m high rock, present halfway between the San Jacinto and Elsinore fault zones (Brune et al., 2006). This rock, along with the other rocks in this area, offers the possibility of obtaining strong statistical constraints on ground motion from large earthquakes along the two faults. Rocks like these provide a direct indication of past ground shaking, as opposed to paleoseismic studies of fault motion, which only indicate total slip in events and not the actual time history of slip. Therefore, these rocks are effectively low-resolution strong motion seismoscopes and have the potential to provide constraints on ground motion for very large historic earthquakes (Brune, 1996; Anoshehpour et al., 2002), and may eventually provide important information for the design of sensitive structures, such as hospitals and power plants.

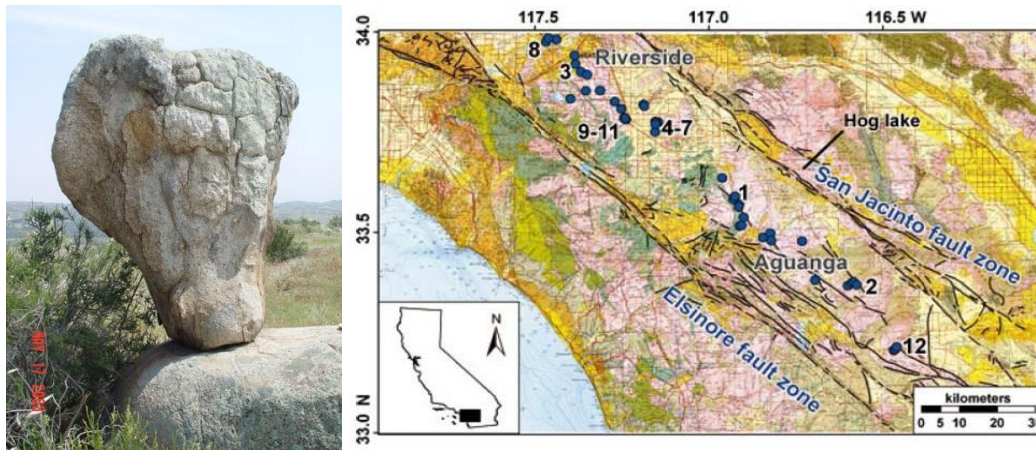


Figure 1.1. Benton Rock and location of band of PBRs between San Jacinto and Elsinore fault zones

Most of the numerical or analytical work on PBRs have roots in Housner's work (Housner, 1963). Housner was among the first to investigate the dynamics of a slender rigid block on a rigid horizontal base undergoing horizontal motion. The governing equations of motion are nonlinear and non-smooth requiring numerical solution or linearization to evaluate the response. Housner linearized the equations of motion and developed an expression for the minimum acceleration required to overturn the block when subjected to two simple base excitations: a rectangular pulse, and a half-sine pulse. Yim et al. (1980) examined the effect of the block size and its slenderness, together with other parameters that affect rocking motion. He found that vertical ground motions and small deviations in the velocity reduction applied at impact (to prevent bouncing when the block transitions from one corner point to another) do not systematically affect the overturning probabilities although they may affect the overturning response in particular cases.

With the advancement in technology, the potential to carry out complex numerical and experimental studies have increased tremendously. Shi et al. (1996) developed a finite-difference numerical code to examine the response of a rocking rigid body subjected to complex ground motions. Zhang and Makris (2001) further discussed the analytical problem and supplemented the results with numerical simulations. Anooshehpour et al. (2004) developed a methodology to obtain the quasi-static toppling acceleration of precariously balanced rocks from field tests. They also conducted shake table experiments on rectangular blocks of various sizes and rocks of different shapes by subjecting them to many synthetic and real ground motion records. They verified that rocking will not initiate unless ground acceleration exceeds the quasi-static toppling acceleration in the case of blocks with simple contacts and they attributed the toppling of a few rocks at accelerations less than quasi-static toppling accelerations to the bumpy contact surface of the rocks. The work of Purvance et al. (2008) is built on the work of Anooshehpour et al. (2004). They inferred that in addition to the block geometrical parameters and PGA, the intensity measures PGV/PGA and the PGA, normalized spectral accelerations at 1 and 2 s [$S_a(1)/PGA$ and $S_a(2)/PGA$] were the strongest indicators of the overturning potential. They also obtained an expression that provides an estimate of the overturning probability, P , based on the PGV/PGA ratio and the slenderness angle, and validated this expression for rectangular blocks and some rocks through various shake table experiments. They idealized the rocks with complex basal contact geometry using models with simple basal points.

These results are a great starting point to understanding precariously balanced rocks even though they have certain limitations. The idealizations and assumptions inherent in these analyses could have a significant impact on their rocking response. Many of the precariously balanced rocks are in locations which are not easily accessible and conducting tilt tests (to obtain quasi-static toppling acceleration) is not feasible. Shake table experiments cannot be performed on the actual rock-pedestal system. A simple 2-D analysis by modifying the rock to resemble a block with simple contact points will not work for all rocks because of two main reasons. Firstly, tilt test data is required for this modification. Secondly, the rocking response of 3-D rocks with complex shapes and complex basal contact points is

not restricted to the plane in which the excitation is applied and we demonstrate in the next section that the basal curvature plays an important role in the response of the rock.

A detailed 3D model of the rock and the pedestal can be built from the data obtained by Terrestrial Laser Scanning (TLS) techniques and also assembled from multi-view photographs of the rocks. The response of this model to different earthquake ground motions can be analyzed using rigid body dynamics under the assumption that the rock and the pedestal behave like rigid bodies. This will provide a good constraint on the upper limit of the ground motions experienced by the site of the rock. We are establishing the proof of concept through a prototype study of the recently imaged Echo Cliffs PBR [Fig. 1.2.] located in the Western Santa Monica Mountains. It lies above the ramp in the fault propagation fold structure that has been interpreted by Davis and Namson as an active structure that may pose a major seismic hazard to the Los Angeles area. The rock withstood moderate ground motions during the 1994 Northridge earthquake. Hudnut et al. (2009) estimate the PGA to have been 0.2g and the PGV to have been 12 cm/sec at this site. The success of the prototype study will provide an impetus to 3-D imaging and analysis of hundreds of PBRs identified and cataloged by Brune et al. (2006).

In this article, we first assess the effect of basal curvature of the rock on the response using idealized version of the Echo Cliff PBR. Then, we develop a methodology to analyze the response of the 3-D rocks using rigid body dynamics. Finally, we validate the methodology using the analytical solution for Housner's block solution as well as an analytical formulation of the idealized version of the Echo Cliff PBR.

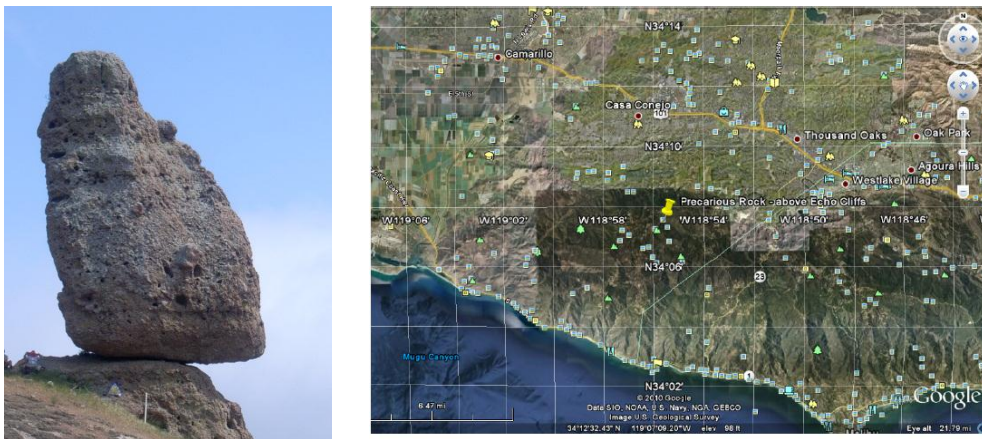


Figure 1.2. Echo Cliff PBR and location of Echo Cliff PBR in Santa Monica Mountains

2. EFFECT OF BASAL CURVATURE

Housner (1963) derived the equation of motion for a rigid rectangular block (with the two corners as contact points) on a rigid base [Fig. 2.1 (a)]. Many others have tried to idealize a 3-D rock with complex basal curvature with a 2-D block supported on two simple contact points [Fig. 2.1 (b)]. Before moving on to the actual rock, it is important to test the effects of basal curvature on the response of the rock in order to judge the accuracy of the simple two point contact approximation. To this end, we have developed an analytical formulation for a rock with an idealized curved base as shown in Fig. 2.2 (a) and (b). The parameters are height of the block (H), radius of curvature of the base (r) and length of flat part on the base of the rock (h). We assume that the block and the ground are rigid, there is no bouncing between rock and pedestal (i.e. at any instant in time at least one point of the block is in contact with the ground), and no sliding between the rock and the pedestal.

This is a single degree of freedom system with the angle rotated by the vector, from the center of arc to the point about which the block initially starts rotating (i.e. the point where the flat part on the base

ends and the arc starts indicated by a thick black arrow in Fig. 2.2 a), of the block (θ) as the degree of freedom. The nonlinear equation of motion, obtained using Lagrangian mechanics, for $0^\circ < \theta < 90^\circ$ is:

$$\ddot{\theta} = \frac{\dot{\theta}}{2I} \frac{dI}{d\theta} - \frac{g}{I} \frac{dA_x}{d\theta} + \frac{a(t)}{I} \frac{dA_y}{d\theta} \quad (2.1)$$

Where, I is the second moment of area about the current contact point, A_x is the first moment of area about the X axis and A_y is the first moment of area about the Y axis, both axes passing through the current contact point. A similar equation can be written for the opposite arc, i.e. $-90^\circ < \theta < 0^\circ$. In order to prevent the bouncing of the block when the response shifts from one arc to the other, conservation of angular momentum is used to derive a relation between the angular velocities just before ($\dot{\theta}_1$) and just after ($\dot{\theta}_2$) transition from one circular arc to another.

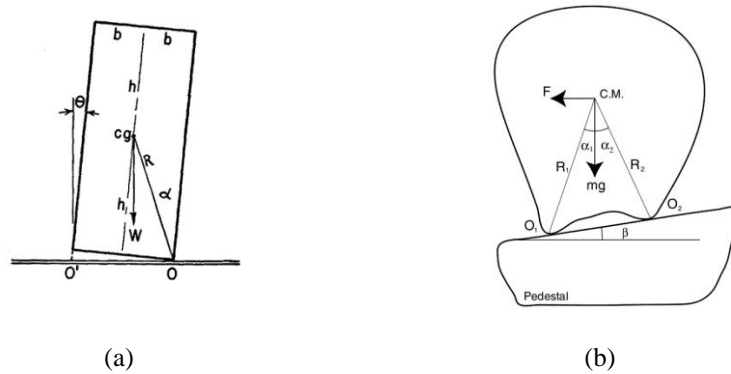


Figure 2.1. (a) Housner's block and (b) simple 2-D approximation of a rock by a two point contact system

To understand the effect of rock basal shape, we estimate the toppling regime of an Echo Cliff PBR-like block by analyzing it under idealized sawtooth-like ground velocity waveforms [Fig. 2.2 (c)] with varying PGV and T. The values of the parameters for the Echo Cliff PBR-like block are $r = 3.62m$, $H = 14.73m$ and $h = 3.38m$. The equation of motion is solved numerically using 4th order Runge-Kutta method. Fragility maps showing the excitation domain where the toppling occurs, are obtained by plotting the peak X displacement of the center of mass as a function of PGV and T of the ground excitation. To analyze the effect of basal curvature, fragility maps are obtained for blocks with $r = 1.81m$, $r = 3.62m$ and $r = 7.24m$ [Fig. 2.3]. As the basal shape factor increases, the excitation domain over which toppling occurs increases. This is the pink region in the Fig 2.3. The fragility maps depend on the value of the peak X displacement of the center of mass. If the center of mass goes beyond a certain point (which depends on the geometrical parameters), the block will topple. Here peak displacement of 5 (pink region in Fig. 4.2.1) indicates the toppling regime of the block.

It can be seen that the basal curvature does have a significant effect on the rocking response. The response of simple two point contact systems would be vastly different from reality. Also the assumptions of no bouncing and no sliding are not very realistic. If either or both phenomena are taken into account, the ground motion required to topple the block would have to be stronger than the analytical case discussed above. This motivates the proposed work of modeling the rocking response (including sliding/bouncing) of precariously balanced rocks in great detail in three dimensions with accurate basal geometry. Fortunately, terrestrial laser-scanning techniques are making it possible to image the outer form of precariously balanced rocks and their contact with the underlying pedestals in unprecedented detail. We are pursuing a method to calculate the 3D response of PBRs that is based on rigid body dynamics incorporating the in-situ contact conditions.

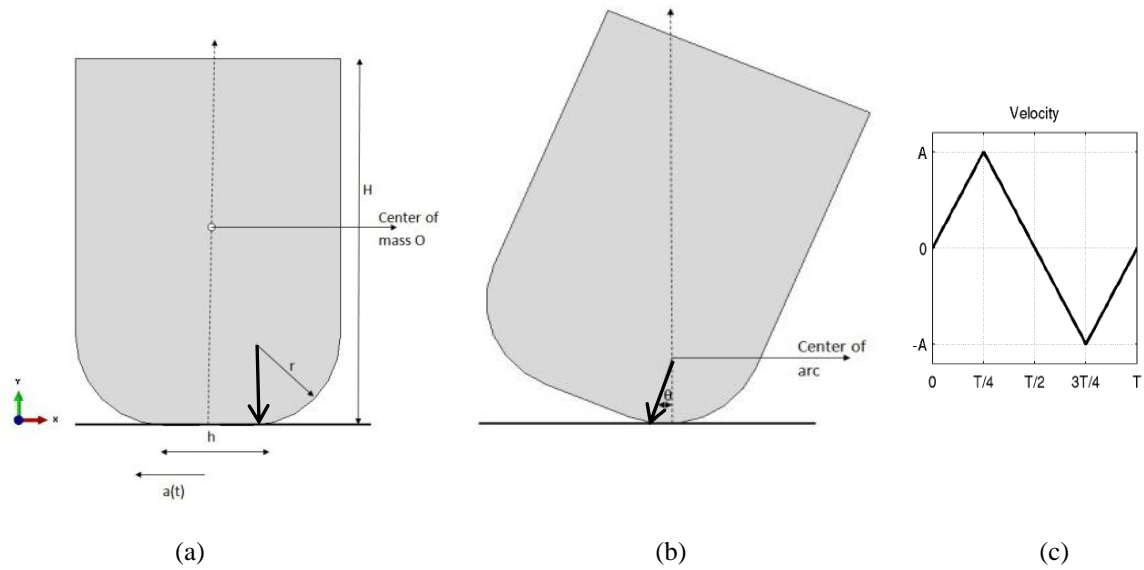


Figure 2.2. (a) Initial configuration of the idealized block with curved base, (b) configuration after it has rotated by an angle θ and (c) idealized saw-tooth ground velocity pulse

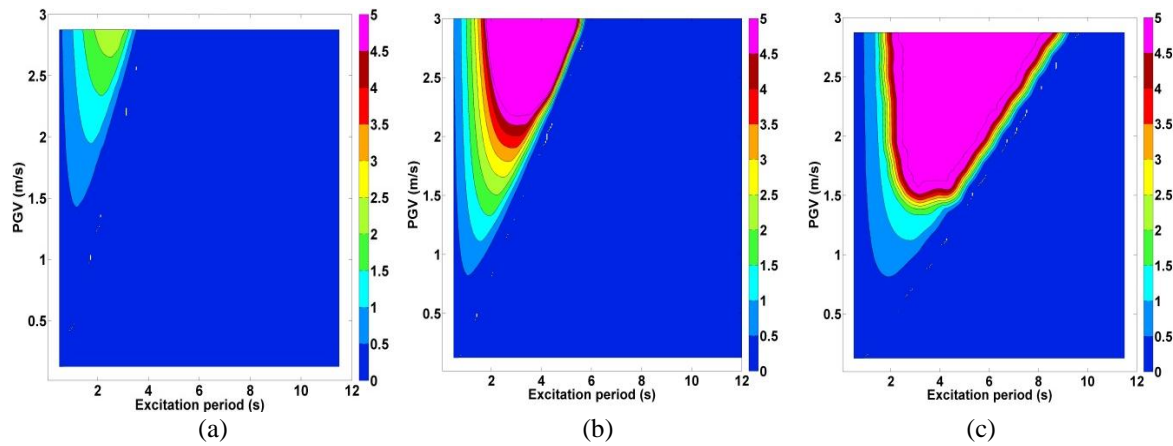


Figure 2.3. Peak X displacement of the center of mass as a function of PGV and T of the ground excitation for (a) basal curvature half that of the rock, (b) basal curvature same as that of the rock and (c) basal curvature twice that of the rock

3. RIGID BODY DYNAMICS

Consider a rigid body rotating and translating in space. XYZ is the global coordinate system attached to the ground and $X'Y'Z'$ is the local coordinate system which is fixed to the rigid body, i.e, the local coordinate system will translate and rotate along with the rigid body. The origin of the local coordinate system is at the center of mass of the body. Initially (at $t=0$), the global and local coordinate systems are co-located. Let \mathbf{u}_{cm} be the position vector of the center of mass in the XYZ coordinate system, $\dot{\mathbf{u}}_{cm}$ be the translational velocity of the center of mass, \mathbf{R} be the rotation matrix which is a transformation mapping from the $X'Y'Z'$ to the XYZ coordinate system and \mathbf{l} be the angular momentum of the rigid body about the center of mass. These four quantities are the state variables as they provide complete set of information about the rigid body at any instant in time. The rate of change of these state variables with respect to time are given by Eqns. 3.1-3.4.

$$\frac{d}{dt} \mathbf{u}_{cm} = \dot{\mathbf{u}}_{cm} \quad (3.1)$$

$$\frac{d}{dt} \dot{\mathbf{u}}_{cm} = \frac{\mathbf{F}_T}{m} \quad (3.2)$$

$$\frac{d}{dt} \mathbf{R} = \boldsymbol{\omega} \times \mathbf{R} \quad (3.3)$$

$$\frac{d}{dt} \mathbf{l} = \boldsymbol{\tau}_T \quad (3.4)$$

Here, \mathbf{I} is the moment of inertia tensor of the body about the center of mass at time t in the XYZ coordinate system, $\boldsymbol{\omega}$ is the angular velocity of the body ($\boldsymbol{\omega} = \mathbf{I}^{-1} \mathbf{l}$), \mathbf{F}_T is the vector of forces acting on the body, $\boldsymbol{\tau}_T$ is the net torque acting on the body and m is the mass of the rigid body. Eqn. 3.2 and Eqn. 3.4 are the force and moment balance equations respectively. Since we assume that the body does not deform, \mathbf{I} needs to be computed just once at $t = 0$. Let \mathbf{I}' be the moment of inertia tensor of the body about the center of mass in the X'Y'Z' coordinate system. \mathbf{I} (at any time t) can be obtained by a simple coordinate transformation ($\mathbf{I} = \mathbf{R}^T \mathbf{I}' \mathbf{R}$).

We can time discretize Eqns. 3.1-3.4 and step forward in time using constant average acceleration method and direct iteration scheme to ensure that equilibrium is satisfied at the end of each time step. At the end of each iteration k when going from t to $t + \Delta t$, we verify whether \mathbf{R}^k is a rotation matrix by checking whether $\det(\mathbf{R}^k) = 1$ and $\mathbf{R}^{kT} \mathbf{R}^k = \mathbf{ID}$, where \mathbf{ID} is the 3×3 identity matrix. If \mathbf{R}^k is not a rotation matrix, then we use Cayley transform (1846) to project \mathbf{R}^k back into $SO(3)$ (Special Orthogonal group, i.e. space of rotational matrices).

The discussion above is for a general rigid body dynamics solver. For the rock, we can use the general solver but for the pedestal we will need only Eqn. 3.1 -3.2 as the pedestal does not rotate. At the end of each time step, we update the coordinates of the nodes on the base of the rock and the nodes on the pedestal and check whether the rock is penetrating into the pedestal. If any of the basal nodes of the rock are within $\pm \varepsilon$ (tolerance) from the surface of the pedestal, then that node of the rock is in contact with the pedestal. If any node of the rock penetrates a distance more than ε into the pedestal, we step back in time and solve the system of equations for a reduced time step. We repeat this procedure until no node of the rock penetrates more than ε into the pedestal.

Once we have the contact points, we need to resolve collisions and find contact forces. Let us consider the case of a ball bouncing on the ground. The instant just before the ball collides with the ground, the relative normal velocity of the ball with respect to the ground is negative, i.e., the ball is moving towards the ground. The instant it hits the ground, the velocity of the ball changes instantaneously and the relative normal velocity of the ball becomes greater than or equal to 0, i.e, it starts moving away from the ground. For changing the velocity of the ball instantaneously, we will have to apply an impulsive force normal to the surface of the ground. The magnitude of the impulsive force will depend on the coefficient of restitution (e) and the state variables. For the case of the rock, say there are q contact points. Let v_i^- and v_i^+ be the relative normal velocity of the rock at the point i , with respect to the pedestal, before and after collision, respectively, and $j_i \mathbf{n}_i$ be the impulse applied at the point. \mathbf{n}_i is the unit normal vector to the pedestal at contact point i . v_i^+ can be written as a linear combination of impulses applied at all contact points. Therefore, $\mathbf{v}^+ = \mathbf{A} \mathbf{j} + \mathbf{b}$ where \mathbf{v}^+ is the vector of relative normal velocities at all contact points after collision and \mathbf{j} is the vector of magnitude of impulsive force at all contact points. Here, A_{mn} contains the contribution of impulse applied at point n to the relative normal velocity at point m and b_m contains the contribution from relative velocity of all the contact points before impact (\mathbf{v}^-). The components of \mathbf{A} are functions of the state variables (\mathbf{u}_{cm}^k , $\dot{\mathbf{u}}_{cm}^k$, \mathbf{R}^k and \mathbf{l}^k), mass of the rock (m), e and \mathbf{I} . Impulses should only push the rock and the pedestal away, they should not make them stick together ($j_i \geq 0$). The relative normal velocities before (v_i^-) and after (v_i^+) collision are related by the coefficient of restitution ($v_i^+ \geq -e v_i^-$). Finally, since the impulse is being applied only to satisfy $v_i^+ \geq -e v_i^-$ at that contact point, if this condition is already

satisfied, the impulse acting at that point should be zero, i.e., $j_i(v_i^+ + e v_i^-) = 0$ (complementarity condition). All these conditions can be put together to form a Linear Complementarity problem (LCP) as shown in Eqn. 3.5. This has been solved using the Dantzig's algorithm (Cottle et al., 1968). Once the impulses are obtained, we update the velocity of the center of mass ($\dot{\mathbf{u}}_{cm}^k$) and the angular momentum (\mathbf{I}^k). For the case of the rock, we can set $e = 0$ if we want the collision to be perfectly inelastic (i.e., no bouncing).

$$\mathbf{v}^+ = \mathbf{A}\mathbf{j} + \mathbf{b}, \quad j_i \geq 0, \quad v_i^+ + e v_i^- \geq 0 \quad \text{and} \quad j_i(v_i^+ + e v_i^-) = 0 \quad (3.5)$$

After resolving collisions, if the relative normal velocity of contact point i is equal to 0, then the point is in resting contact. For example, a book resting on a table or sliding on a table are examples of resting contact. For each contact point, along with the normal direction, we define a set of orthogonal vectors (\mathbf{x}_i and \mathbf{y}_i) which are tangential to the surface of the pedestal. \mathbf{x}_i , \mathbf{y}_i and \mathbf{n}_i form an orthogonal coordinate system at contact point i . Let a_{ni} , a_{xi} and a_{yi} be the relative normal and tangential accelerations of point i on the base of the rock with respect to the pedestal. Whereas in case of collision, we apply impulses in order to change the velocities, for resting contact, we modify the acceleration of the body so that it does not penetrate into the pedestal. We do this by applying normal contact forces ($f_{ni}\mathbf{n}_i$) at each contact point. In order to model the effects of friction between the rock and the pedestal, we apply tangential frictional forces ($f_{xi}\mathbf{x}_i$ and $f_{yi}\mathbf{y}_i$). If the relative tangential velocity of the contact point i is zero, then we have the case of static friction, otherwise we have the case of dynamic friction.

Let us consider the case where there is only static friction. Let μ_s and μ_d be the coefficient of static and dynamic friction respectively. Let $\mathbf{a} = \langle a_{n1} \ a_{x1} \ a_{y1} \ \dots \ a_{ni} \ a_{xi} \ a_{yi} \ \dots \ \rangle^T$ and $\mathbf{f} = \langle f_{n1} \ f_{x1} \ f_{y1} \ \dots \ f_{ni} \ f_{xi} \ f_{yi} \ \dots \ \rangle^T$. Similar to the approach taken to resolve collision, the acceleration of any point i can be written as a linear combination of the forces acting on all the contact points. Therefore, $\mathbf{a} = \mathbf{A}\mathbf{f} + \mathbf{b}$. Here, \mathbf{A} and \mathbf{b} are functions of the state variables, mass of the rock and the moment of inertia tensor. A_{mn} represents the contribution of force acting at point m to the acceleration at point n and b_m represents the contribution of external forces like gravity to the acceleration of point m . The normal forces can only push the bodies apart and cannot pull them together, i.e., $f_{ni} \geq 0$. If the relative normal acceleration of a contact point is negative, the point will penetrate into the pedestal during the next step. So, we want the relative normal accelerations to be greater than or equal to zero, i.e., $a_{ni} \geq 0$. If the relative normal acceleration of a contact point is greater than zero, it implies that the point will move away from the pedestal during the next time step, therefore, the normal contact force acting on it should be zero, i.e., $f_{ni}a_{ni} = 0$. The conditions on the frictional force are: (i) its magnitude at a point should be less than $\mu_s f_{ni}$, (ii) it should partially oppose the tangential acceleration, i.e., $f_{xi}a_{xi} + f_{yi}a_{yi} \leq 0$ and (iii) if the magnitude of the tangential acceleration is greater than zero, during the next iteration the rock can start sliding, therefore, it should be at its maximum value ($\mu_s f_{ni}$). The LCP is given in Eqns. 3.6 and 3.7. Baraff(1994) modified Dantzig's algorithm to incorporate frictional forces for a 2-D problem. We have modified that algorithm to accommodate friction in a 3-D problem.

$$\mathbf{a} = \mathbf{A}\mathbf{f} + \mathbf{b}, \quad f_{ni} \geq 0, \quad a_{ni} \geq 0 \quad \text{and} \quad f_{ni}a_{ni} = 0 \quad (3.6)$$

$$\sqrt{f_{xi}^2 + f_{yi}^2} \leq \mu f_{ni}, \quad f_{xi}a_{xi} + f_{yi}a_{yi} \leq 0 \quad \text{and} \quad \sqrt{a_{xi}^2 + a_{yi}^2} \left(\mu f_{ni} - \sqrt{f_{xi}^2 + f_{yi}^2} \right) = 0 \quad (3.7)$$

When the rock starts sliding (i.e., when relative tangential velocity of the contact points are non-zero), there will be dynamic friction involved in the problem. The frictional force will have the magnitude of $\mu_d f_{ni}$ and the direction of force is such that it opposes the tangential velocity. Once the contact forces are obtained, we can include these forces into the \mathbf{F}_T^k and the moments due to these forces into $\boldsymbol{\tau}_T^k$, solve the system of Eqns. 3.1-3.4 for the next time step, and march forward in time.

4. VALIDATION OF RIGID BODY DYNAMICS ALGORITHM

We will now validate the rigid body dynamics algorithm for two cases: uni-directional ground acceleration (Housner's block subjected to half sine pulse) and bi-directional ground acceleration (idealized Echo Cliff Rock-like block subjected to idealized sawtooth ground velocity pulse).

4.1 Housner's block

We first validate the rigid body dynamics algorithm using the Housner's block solution. Housner (1963) linearized the equation of motion, applied a half-sine pulse acceleration to a rigid rectangular block sitting on a rigid surface and calculated an expression for the magnitude of acceleration required to topple the block. We solve the nonlinear equation of motion for the Housner's block using 4th order Runge-Kutta method and compare this solution against computed by the rigid body dynamics algorithm.

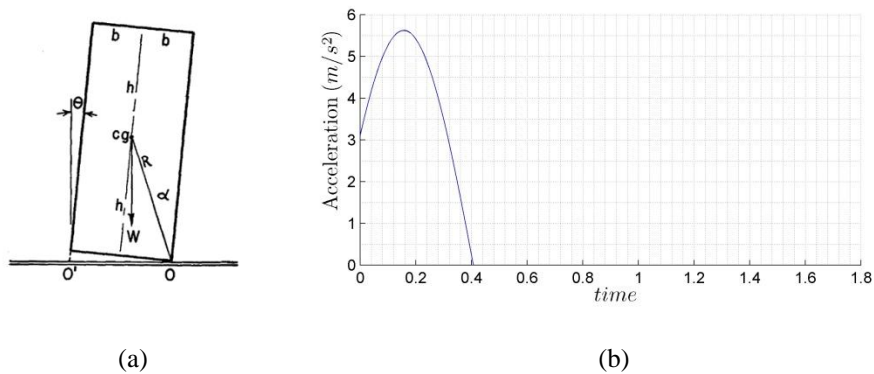


Figure 4.1.1. (a) Housner's block and (b) Half sine-pulse acceleration

The parameters of the block are half width (b) = 0.2 m, half height (h) = 0.6 m and angular frequency of ground excitation (ω) = 2π rad/sec. The acceleration applied is $a \sin(\omega t + \varphi)$ [Fig. 4.1.1(b)], where a is the magnitude of applied excitation, ω is the angular frequency of ground excitation and φ is the phase angle (which is such that the acceleration at $t=0$ is just enough for the block to lift off the ground). Both the methods predict the magnitude of toppling acceleration to be between $5.62 - 5.64 m/s^2$ (note the load step size for computation is $0.02 m/s^2$). The time history of the angular displacement of the block (θ) normalized by the slenderness angle [$\alpha = \tan^{-1}(b/h)$] is plotted for $a = 5.62 m/s^2$ and $a = 5.64 m/s^2$ [Fig. 4.1.2]. The toppling criterion is that if $\theta/\alpha > 1$, then the block topples as the applied acceleration is unidirectional.

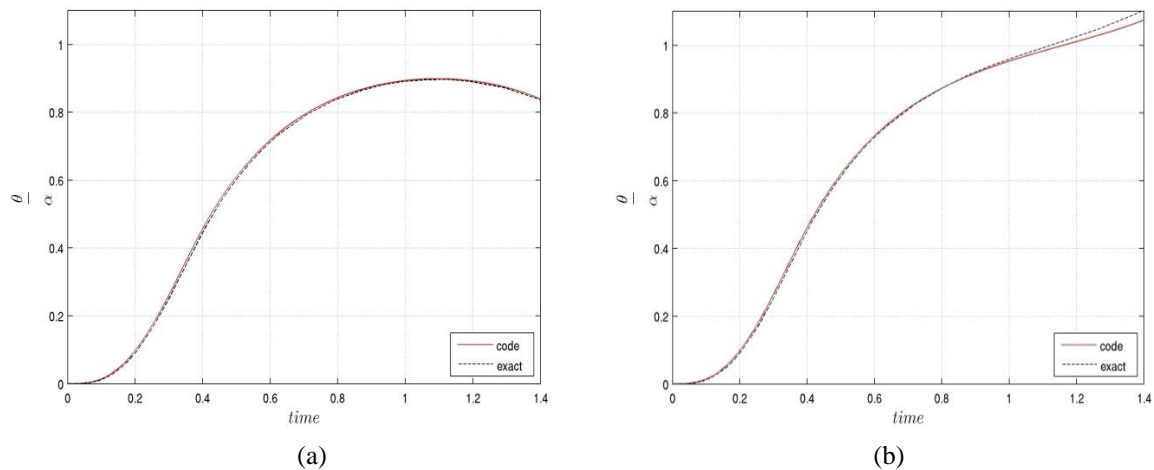


Figure 4.1.2. Normalized angular rotation time history for (a) $a = 5.62 m/s^2$ (Non-toppling case) and (b)

$$a = 5.64 \text{ m/s}^2 \text{ (Toppling case)}$$

4.2. Idealized Echo Cliff-like block

Next we validate the algorithm using the results from the idealized representation of the Echo Cliff rock [Fig. 2.2 (a) and (b)]. Recall that, in section 2 we presented the equation of motion for an idealized block with basal curvature and obtained the fragility maps under idealized sawtooth type ground velocity pulse [Fig. 2.2 (c)] by solving Eqn. 2.1 using 4th order Runge-Kutta method. The fragility maps depend on the value of the peak X displacement of the center of mass. If the center of mass goes beyond a certain point (which depends on the geometrical parameters), the block will topple. Here peak displacement of 5 (pink region in Fig. 4.2.1) indicates the toppling regime of the block.

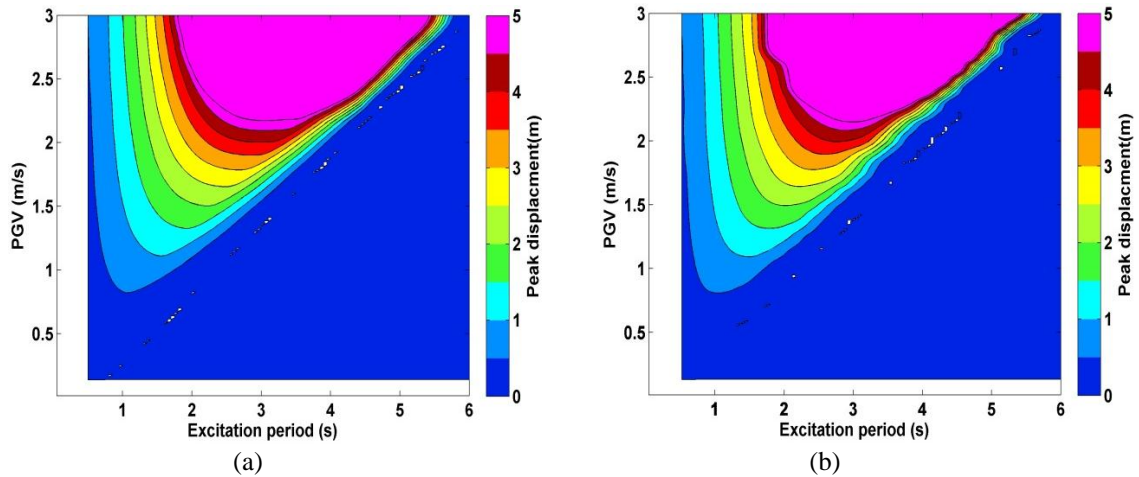


Figure 4.2.1. Fragility maps for idealized Echo Cliff-like block as a function of PGV and T for sawtooth type ground velocity pulse using (a) analytical method presented in section 2 and (b) rigid body dynamics algorithm

5. Modeling Echo Cliff PBR and Future Work

As a first step to modeling the rock, we need to find the moment of inertia tensor of the rock about its center of mass. The Echo Cliff PBR was imaged by Hudnut et al. (2009) using TLS (Terrestrial Laser Scanning) techniques. The point cloud obtained from TLS is very dense [Fig. 5.1]. To reduce the computational effort, we select a reduced data-cloud consisting of 864 points, with 624 points on the rock and 240 points on the pedestal. The points on the rock represent only the outer surface of the rock and they are not equally spaced. In order to obtain equally spaced nodes throughout the rock, a delaunay tetrahedralization of the rock is created using MATLAB. A 3D grid of equally spaced points is created and all the points which lie on or inside any of these tetrahedrons form the equally spaced nodes of the rock [Fig. 5.1]. Assuming that the density of the rock is constant, we calculate the moment of inertia tensor of the rock using the coordinates of the nodes. To determine the rock-pedestal interface points, the dense data cloud of the interface obtained from the TLS data is superimposed on the nodes present at the base of the rock and the nearest neighbors to the interface data cloud are found. Any node on the base which is on or inside the boundary specified by the interface data cloud constitutes a basal contact point. Assuming that the density of the rock does not vary, we can calculate the moment of inertia tensor of the rock from the nodal positions.

We are currently analysing the response of the rock to idealized ground velocity pulse [Fig. 2.2 (c)] applied in different directions and we plan to compare the results obtained from this analysis with that obtained by Purvance et al. (2008), who obtained a generalized expression for the overturning probability from a series of shake table experiments on blocks of varying sizes. We will then examine the effect of sliding by varying the coefficient of friction. From a thorough analysis of the Echo Cliff

PBR, we are trying to assess the toppling sensitivity of the rock to the pulse period, amplitude, number of cycles, direction of excitation and coefficient of friction. We will then analyze the other rocks present in Southern California and come up with probabilistic constraints on region-wide ground shaking intensity for Southern California.

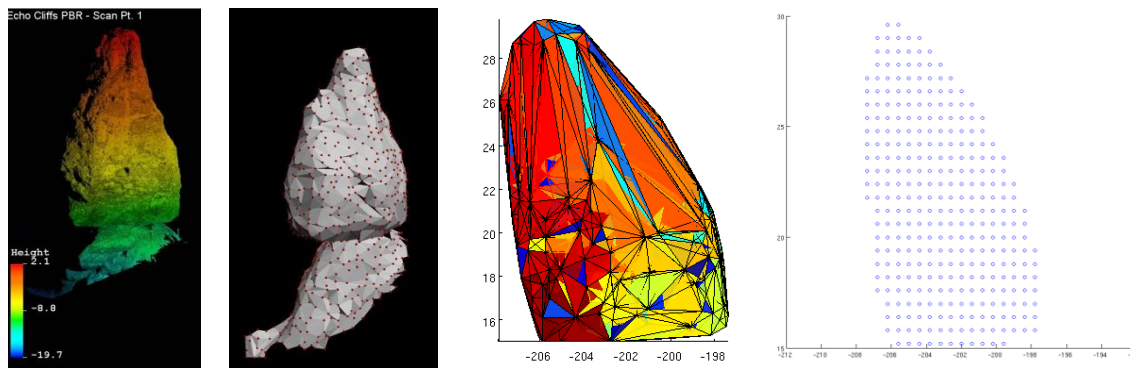


Figure 5.1. Dense point cloud from TLS data, coarser set of nodes, delaunay triangulation using MATLAB and equally spaced nodes of the rock

ACKNOWLEDGEMENT

We acknowledge the Southern California Earthquake Center (SCEC) and the United States Geological Survey (USGS) for funding this project. We thank Dr. Hudnut for providing us with the data for the Echo Cliff PBR.

REFERENCES

- Anooshehpour, A., and Brune, J.N. (2002). Verification of precarious methodology using shake table tests of rocks and rock models. *Soil Dynamics and Earthquake Engineering* **22**, 917-922.
- Anooshehpour, A, Brune, J.N., and Zeng, Y. (2004). Methodology for obtaining constraints on ground motion from precariously balanced rocks. *Seismological Society of America Bulletin* **94:1**, 285-303.
- Baraff, D. (1994). Fast contact force computation for nonpenetrating rigid bodies. *Computer Graphics Proceedings (SIGGRAPH)*
- Bell, J.W., Brune, J.N., Liu, T., Zerda, M., and Yount, J.C. (1998). Dating the precariously balanced rocks in seismically active parts of California and Nevada. *Geology* **26**, 495-498.
- Brune, J.N., Precariously balanced rocks and ground motion maps for southern California. *Seismological Society of America Bulletin* **86:1A**, 43-54.
- Brune, J.N., Anooshehpour, A., Purvance, M.D., and Brune, R.J. (2006). Band of precariously balanced rocks between Elsinore and San Jacinto, California, fault zones: Constraints on ground motions for large earthquakes. *Geology* **34:3**, 137-140.
- Cayley, A. (1846). Sur quelques propriétés des déterminants gauches. *Journal für die Reine und Angewandte Mathematik* **32**, 119-123.
- Cottle, R., and Dantzig, G. (1968). Complementary pivot theory of mathematical programming. *Linear Algebra and its Applications* **1**, 103-125.
- Housner, G.W. (1963). The behavior of inverted pendulum structures during earthquakes. *Bulletin of the Seismological Society of America* **53:2**, 403-417.
- Hudnut, K. W., Amidon, W., Bawden, G., Brune, J., Bond, S., Graves, R., Haddad, D.E., Limaye, A., Lynch, D.K., Phillips, D.A., Pounders, E., and Rood, D. (2009). The Echo Cliffs precariously balanced rocks: Discovery and Terrestrial Laser Scanning. *American Geophysical Union Fall meeting*.
- Purvance, M., Anooshehpour, A., and Brune, J.N. (2008). Freestanding block overturning fragilities: Numerical simulation and experimental validation. *Earthquake Engineering and Structural Dynamics* **37**, 791-808.
- Shi, B., Anooshehpour, A., Zeng, Y., and Brune, J.N. (1996). Rocking and overturning of precariously balanced rocks by earthquakes. *Seismological Society of America Bulletin* **86**, 1364-1371.
- Yim, C., Chopra, A.K., and Penzien, J. (1980). Rocking response of rigid blocks to earthquakes. *Earthquake Engineering and Structural Dynamics* **8**, 565-587.
- Zhang, J., and Makris, N. (2001). Rocking response of free-standing blocks under cycloidal pulses. *Journal of Engineering Mechanics* **127**, 473-483